New Journal of Physics
The open-access journal for physics

Coherent broadband continuous-wave terahertz spectroscopy on solid-state samples

A Roggenbuck[1,2], H Schmitz[1], A Deninger[2], I Cámara Mayorga[3], J Hemberger[1], R Güsten[3] and M Grüninger[1,4]

[1] II. Physikalisches Institut, Universität zu Köln, Zülpicher Strasse 77, D-50937 Köln, Germany
[2] TOPTICA Photonics AG, Lochhamer Schlag 19, D-82166 Gräfelfing, Germany
[3] Max-Planck-Institute for Radio Astronomy, Auf dem Hügel 69, D-53121 Bonn, Germany
E-mail: grueninger@ph2.uni-koeln.de

New Journal of Physics **12** (2010) 043017 (13pp)
Received 21 September 2009
Published 13 April 2010
Online at http://www.njp.org/
doi:10.1088/1367-2630/12/4/043017

Abstract. Measuring the complex dielectric function $\varepsilon(\omega) = \varepsilon_1 + i\varepsilon_2$ of solid-state samples in the terahertz frequency range with high spectral resolution remains difficult. Using a continuous-wave terahertz spectrometer based on photomixing in the frequency range from 60 GHz to 1.8 THz, we obtain the most precise data of $\varepsilon(\omega)$ reported to date for the well-studied example of α-lactose monohydrate. We are able to determine both ε_1 and ε_2 due to coherent detection and show that the results are Kramers–Kronig consistent. Our analysis is based on scanning an interference pattern in frequency and relies on the high spectral resolution in the MHz range. This enables us to avoid mechanically moving parts such as a delay stage. Moreover, we show that the optical data can be used to determine both $\varepsilon(\omega)$ and the sample thickness d independently.

[4] Author to whom any correspondence should be addressed.

Contents

1. Introduction

Spectroscopy in the terahertz frequency range has developed rapidly in recent years. In particular, terahertz time-domain spectroscopy has become a common tool. The alternative of measuring in the frequency domain with a continuous-wave technique offers the advantages of frequency selectivity and a much higher frequency resolution [1, 2]. Typical linewidths in solid-state samples are of the order of several tens of GHz or broader; thus a spectral resolution of a few GHz is usually sufficient. However, a central problem for solid-state spectroscopy is that both the real and the imaginary part of the complex dielectric function $\varepsilon(\omega) = \varepsilon_1 + \mathrm{i}\varepsilon_2$ or, equivalently, of the complex refractive index $n + \mathrm{i}k$ have to be determined reliably, e.g. by measuring both the amplitude and the phase of the terahertz radiation. In the frequency domain, very high frequency stability and spectral resolution offer the possibility of determining the phase accurately without any mechanically moving parts (see below). Technically, achieving a high resolution in combination with a broad frequency range is particularly demanding.

One method of generating continuous-wave (cw) terahertz radiation is optical heterodyne conversion or photomixing: the combined output of two lasers illuminates a photoconductive switch integrated into an antenna structure [3]. Applying a bias voltage then leads to the emission of electromagnetic radiation from the antenna at the difference frequency of the two lasers.

Determination of the phase requires a coherent detection scheme, using e.g. a second photomixer as a detector [4]. This second photomixer is illuminated simultaneously by the terahertz beam and by the same two-frequency laser source as the first photomixer. The resulting photocurrent $I_{\mathrm{ph}} \propto E_{\mathrm{THz}} \cos(\Delta\varphi)$ depends both on the amplitude of the terahertz electric field E_{THz} and on the phase difference $\Delta\varphi$ between the terahertz radiation and the laser beat signal.

Varying the phase difference $\Delta\varphi$ with a variable delay stage [5] is one possibility for determining both amplitude and phase for a given frequency. Such a mechanical modulation of the terahertz path is rather slow and the optical data may deteriorate, e.g. due to standing waves or if the terahertz beam is not perfectly collimated. As an alternative, the terahertz phase can be controlled via electro-optical modulation of the phase of one of the two lasers [6, 7]. However, the laser wavelength is orders of magnitude smaller than the terahertz wavelength; therefore this technique is much more sensitive to e.g. thermal drifts of the optical path length.

By contrast, our analysis is based on *scanning an interference pattern in frequency*, exploiting the fact that the period of the interference pattern can be chosen to be much smaller than even the most narrow lines in a solid-state sample. Here, we show that this approach is very well suited for solid-state spectroscopy, yielding precise and reliable values of both $\varepsilon_1(\omega)$ and $\varepsilon_2(\omega)$ without making use of any mechanically moving parts.

The determination of the refractive index n of a solid-state sample based on photomixing and coherent detection has been reported for fused silica [8] and teflon [9], but in both cases n has been determined only for a few distinct frequencies, and the analysis employed a variable delay stage. A comparison of scanning the frequency for a fixed delay versus scanning the delay for a fixed frequency has been reported by Mouret *et al* [10] more recently. However, they used the former technique only to measure the thickness d of a sample for a *given* value of the refractive index n. Here, we show that the optical data suffices to determine both $n(\omega)$ and d independently.

We have chosen α-lactose monohydrate ($C_{12}H_{22}O_{11}$) as an example because it displays a series of narrow absorption lines in the terahertz range, which have been studied in the literature using different techniques, both in the time domain and in the frequency domain [11]–[18]. These reports partly disagree with each other on the center frequency and on the linewidth. Our results on ε_1 and ε_2 are described very well by a Drude–Lorentz model; thus they are Kramers–Kronig consistent with one other.

2. Experimental setup

Our cw terahertz spectrometer employs two distributed-feedback diode lasers, which are tunable around 853 and 855 nm, respectively. Using interferometric frequency control, the setup achieves both a spectral resolution and a long-term frequency stability on the MHz level [5]. It thus offers adequate conditions for the precise determination of the phase. The upper limit of the difference frequency is obtained by cooling the first laser diode close to 0 °C while heating the second one to 50 °C, reaching the limits of the mode-hop-free tuning range. The laser beat can thus be varied continuously from 0 to 1.8 THz. The low-frequency limit of the spectrometer of about 60 GHz is set by the photomixers and by problems in the analysis arising due to standing waves (see below). The superimposed laser beams are fed into a tapered amplifier (Toptica BoosTA 850). This semiconductor amplifier serves to amplify the two-color laser light while maintaining the spectral properties, in particular the linewidth and tunability. An input power of 40 mW is amplified to a free-space output of above 500 mW. After 60 dB optical isolation and coupling into a fiber-optical 50:50 splitter, we still obtain $\geqslant$100 mW power at each of the two fiber outputs. These outputs are connected to the fiber-pigtailed photomixers, i.e. to the terahertz source and detector, respectively (see figure 1).

We use a new generation of terahertz sources and detectors that are made up of high-energy ion-implanted GaAs interdigitated photomixers with a mixing area of about $9 \times 9\,\mu m^2$ [19]. In comparison to low-temperature-grown GaAs, the advantage of ion implantation is that it yields a highly reproducible photoconductive material. The photomixers are integrated within self-complementary log-periodic spiral broadband antennae with three turns. The design is chosen to obtain a nearly constant antenna impedance in the frequency range above about 100 GHz. In order to suppress back-reflections and for pre-collimation, the terahertz radiation is coupled to free space via a hyperhemispherical silicon lens. The residual beam divergence is $<10^\circ$ full-width at half-maximum (FWHM). The emitted terahertz radiation is collimated and

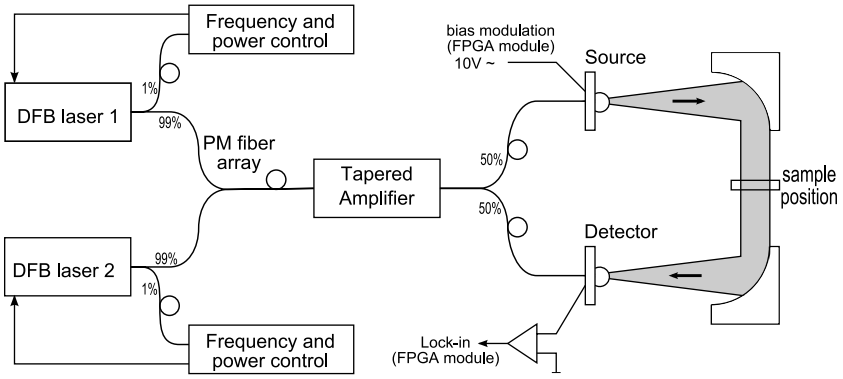

Figure 1. Setup of the cw terahertz spectrometer.

then focused onto the detector by two off-axis parabolic mirrors (focal length $f = 75$ mm; see figure 1). The sample is placed on an aperture in the collimated beam.

The photocurrent in the detector is smaller than 1 μA, and in the vicinity of an absorption band of the sample or in the case of destructive interference (see below) the photocurrent may become as small as the noise level of about 4 pA. Therefore, the signal is pre-amplified by a transimpedance amplifier and we use a lock-in technique. Modulation of the bias voltage of the source photomixer ($U_{AC} \sim 10$ V, modulation frequency up to 10 kHz) and lock-in detection of the pre-amplified signal of the second photomixer are realized by a digital lock-in module (Toptica TeraControl 110)[5] based on a field-programmable gate array (FPGA).

3. Signal-to-noise performance

The power P_{THz} of the terahertz radiation and the detected photocurrent I_{ph} in the receiver photomixer are related by $P_{THz} \propto I_{ph}^2$. Thus the dynamic range in dB equals $20 \log_{10}(I_{ph}/I_{noise})$, where I_{noise} denotes the noise photocurrent measured with a blocked terahertz beam, and I_{ph} refers to a measurement without a sample. With a modulation frequency of around 5 kHz, we measure $I_{noise} \approx 4$ pA independent of the terahertz frequency. The lock-in averaging time used here is 300 ms and the data acquisition rate, considering some software overlap, is around 3 Hz. As far as the signal is concerned, the detected photocurrent I_{ph} varies with frequency due to the photomixer efficiency. We obtain $I_{ph} > 100$ nA at 100 GHz and $I_{ph} \leqslant 0.5$ nA at 1.8 THz. We thus achieve a dynamic range of up to $\sim$90 dB at 100 GHz and $\sim$40 dB at 1.8 THz. The frequency dependence is plotted in figure 2; it clearly demonstrates the suitability of our setup for spectroscopy, showing distinctive narrow absorption features due to water vapor in the terahertz beam.

[5] The output filter of the lock-in amplifier is a resettable digital integrator that is synchronized with the terahertz frequency control. The integrator thus re-starts as soon as the system is tuned to a new terahertz frequency. This is a substantial advantage in comparison to a conventional analogue RC low-pass filter because the analogue filter requires a waiting time of several time constants. The integration times given here can be roughly three times larger at the same overall measurement speed. To minimize statistical errors, the integration times, ranging from 20 to 600 ms, are chosen to be an exact multiple of the modulation period, which is a further advantage over a conventional analogue RC low-pass filter.

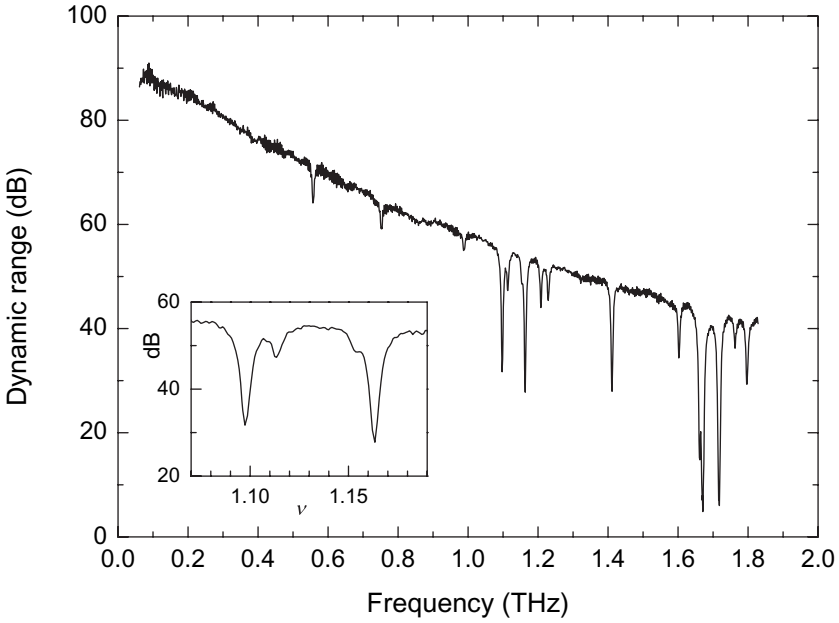

Figure 2. Dynamic range of the terahertz power in the frequency range from 60 GHz to 1.83 THz. The narrow absorption features of water vapor correspond to the spectrum of about 35 cm of air. Absorption lines are clearly resolved at 557, 752, 988, 1097, 1113, 1163, 1208, 1229, 1411, 1602, 1661, 1669, 1717, 1762 and 1795/1797 GHz, in agreement with [20]. Inset: some absorption lines on an enlarged scale.

4. Data analysis

The detected photocurrent I_{ph} depends on the amplitude of the terahertz electric field, E_{THz}, and on the phase difference $\Delta\varphi$ between the terahertz wave and the laser beat signal:

$$I_{\mathrm{ph}} \propto E_{\mathrm{THz}} \cos(\Delta\varphi) = E_{\mathrm{THz}} \cos(2\pi\, \Delta L\, \nu/c), \tag{1}$$

where ν denotes the terahertz frequency, c is the speed of light, and

$$\Delta L = (L_{\mathrm{S}} + L_{\mathrm{THz}}) - L_{\mathrm{D}} \tag{2}$$

is the difference between the optical path L_{D} traveled by the laser beat to the detector, on the one hand, and the optical path L_{S} of the laser beat to the terahertz source plus the terahertz path L_{THz} from the source to the detector, on the other. One possible way to separate the amplitude and phase of the terahertz signal for any given frequency is to vary L_{THz} and thus ΔL with the help of a variable delay stage [5], [8]–[10]. Alternatively, the phase difference $\Delta\varphi$ can be varied by scanning the terahertz frequency ν, which has the significant advantages of avoiding any mechanically moving parts and of a much higher scanning rate (up to 10 Hz, depending on the selected lock-in time, but limited by software overlap). In this case, the detected photocurrent I_{ph} oscillates with frequency (see figure 3), and the oscillation period is set by the choice of ΔL. For the case of the reference measurement without a sample, the terahertz beam travels through air with a refractive index of $n_{\mathrm{air}} \approx 1$ independent of frequency; thus $\Delta L^{\mathrm{ref}} = \mathrm{const}$, and the

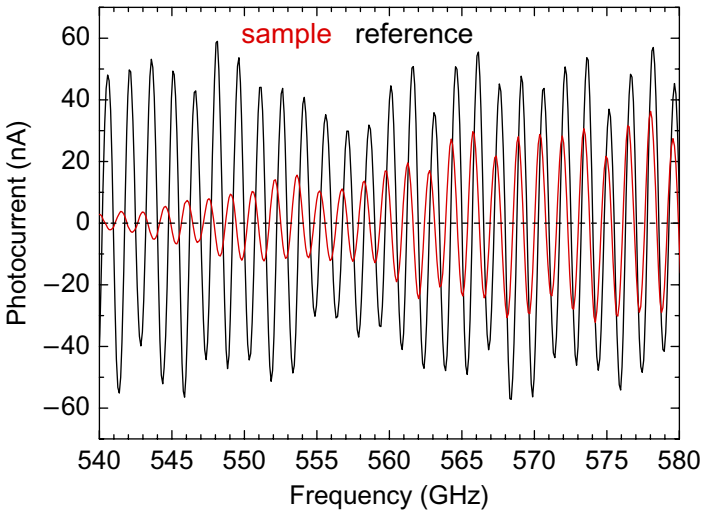

Figure 3. An example of the detected terahertz photocurrent with and without the lactose sample. Both amplitude and phase information can be derived (see the text). The period $\Delta\nu$ of the interference pattern depends on the optical path difference ΔL (see equation (1)). Here, $\Delta\nu \approx 1.5\,\mathrm{GHz}$ and $\Delta L \approx 0.2\,\mathrm{m}$. The suppression of the signal around 557 GHz is due to a water absorption line.

maxima $\nu^{\mathrm{ref}}_{\mathrm{max},m}$ of order $m = 1, 2, 3, \ldots$ are equally spaced in frequency

$$\nu^{\mathrm{ref}}_{\mathrm{max},m} = m\frac{c}{\Delta L^{\mathrm{ref}}}, \tag{3}$$

where ΔL^{ref} denotes the optical path difference (see equation (2)) in the case of the reference measurement. This interference pattern can also be used as a precise test or reference for the actual terahertz frequency.

In comparison to the reference measurement, the sample with refractive index n and thickness d changes the terahertz path L_{THz} by $(n - n_{\mathrm{air}})d$, where we have assumed that the light passes the sample only once, i.e. neglecting multiple reflections within the sample. The sample thus shifts the interference pattern. As an example, figure 3 shows the detected photocurrent in the frequency range just above one of the absorption lines of lactose. This plot clearly demonstrates how the interference pattern of the sample data shifts with respect to the reference data from out-of-phase at 540 GHz to in-phase at 580 GHz. The phase information can be gained most accurately from both the extrema and the zero crossings of I_{ph}, yielding a frequency resolution of the phase data of 1/4 period of the interference pattern, i.e. $c/(4 \times \Delta L)$. Thus the spectral resolution of the phase can be adapted easily by varying the optical path difference ΔL (see equation (2)). An enhancement of the spectral resolution, however, requires a larger density of data points, which increases the total measurement time.

An interference maximum of order m occurs for $\Delta L = m \times c/\nu$. Comparing reference and sample data, the refractive index can be calculated according to

$$(n - n_{\mathrm{air}})d = \left(\frac{\nu^{\mathrm{ref}}_{\mathrm{max},m}}{\nu^{\mathrm{sam}}_{\mathrm{max},m}} - 1\right)\Delta L^{\mathrm{ref}}, \tag{4}$$

where $\nu^{\mathrm{ref}}_{\mathrm{max},m}$ and $\nu^{\mathrm{sam}}_{\mathrm{max},m}$ denote the frequencies of the maxima of order m of the reference and the sample measurement, respectively. In the following, we assume $n_{\mathrm{air}} = 1$. In the case of the reference data, determination of the order m is straightforward because the maxima are equally spaced in frequency, see equation (3). Owing to the frequency dependence of n, the order of the maxima may be ambiguous in the sample data if only a narrow frequency range is explored. However, analyzing the broad frequency range accessible to our spectrometer, the possible ambiguity can be easily removed. Finally, determination of the absolute value of n requires knowledge of the sample thickness d, which can be obtained independently from the measured amplitude (see below).

We emphasize that the refractive index $n(\omega)$ can in principle be determined entirely independently of possible fluctuations of the intensity if the zero crossings of I_{ph} are used for the determination of the phase. The central prerequisite for a precise determination of $n(\omega)$ is the stability of the frequency.

In addition to changing the optical path length, the sample partly absorbs the terahertz light, according to its extinction coefficient $k(\omega)$. The transmittance $T(\omega)$ can be determined by comparing the envelopes of the sample data and of the reference data,

$$T = \left(\frac{I^{\mathrm{sam}}_{\mathrm{ph}}}{I^{\mathrm{ref}}_{\mathrm{ph}}} \right)^2 , \tag{5}$$

where $I^{\mathrm{sam}}_{\mathrm{ph}}$ and $I^{\mathrm{ref}}_{\mathrm{ph}}$ denote the detected photocurrents of the sample and reference data at the extrema of the respective interference patterns (the sample data are interpolated on the equally spaced frequency grid of the extrema of the reference data). Using only the extrema, the effective frequency resolution for the amplitude is $c/(2 \times \Delta L)$, e.g. 0.5 GHz for $\Delta L = 0.3$ m, well beyond the typical requirements for solid-state spectroscopy.

In contrast to the predictions of equation (1), the reference data show deviations from a perfect cosine, see figure 3. These deviations are mainly caused by standing waves within the setup, but absorption of e.g. water vapor also has to be considered. Standing waves originate from multiple reflections, e.g. within the Si lenses of the photomixers, yielding a modulation period of several GHz. If the sample and reference are compared at exactly the same frequency, i.e. if the extrema of order m of the reference data and order m' of the sample data coincide, $\nu^{\mathrm{ref}}_{\mathrm{max},m} = \nu^{\mathrm{sam}}_{\mathrm{max},m'}$, the effect of the parasitic modulations cancels out in the transmittance spectrum. However, if the positions of the extrema differ between the sample and reference scans, then the parasitic modulation diminishes the accuracy of the transmittance data. This effect can be reduced by choosing a smaller period for the interference pattern.

Some of the standing waves are influenced or caused by the sample itself, e.g. standing waves between the terahertz source and the terahertz detector or between one of the photomixers and the sample. These do not cancel out when the sample and reference are compared. Finally, there can be standing waves *within* the sample itself. These can be used to determine the refractive index n and the sample thickness d independently, as discussed in the following paragraph.

5. α-Lactose monohydrate

As a test sample, we utilized commercially available α-lactose monohydrate powder, which we compressed to pellets of 1.3 cm diameter with parallel surfaces by applying a pressure

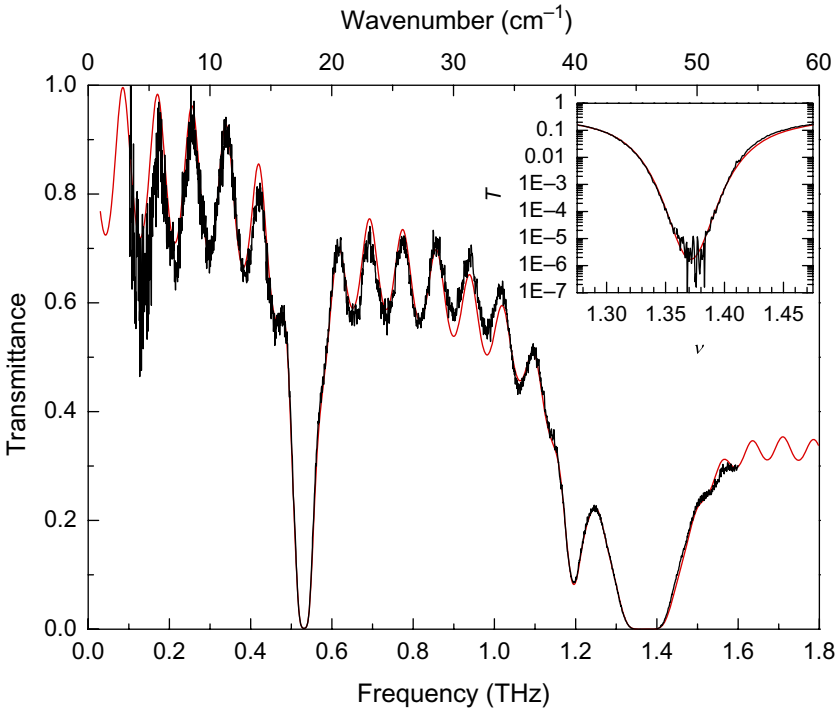

Figure 4. Transmittance $T(\omega)$ of α-lactose monohydrate for a thickness of $d \approx 1$ mm. Three absorption lines are observed at 0.530, 1.195 and 1.369 THz. For large values of T, multiple reflections within the sample give rise to Fabry–Perot interference fringes. The red line depicts a fit according to the Drude–Lorentz model. Inset: $T(\omega)$ around the absorption feature at 1.369 THz, plotted on a log scale.

of about 5 kbar for 1 min. The samples were placed on an aperture with 1 cm diameter, and we used the empty aperture for reference measurements. This normalization eliminated the signatures of water vapor present in the raw data. The transmittance of a pellet with a thickness of $d = (0.98 \pm 0.01)$ mm is depicted in figure 4. The data are shown only up to 1.6 THz due to the strong absorption lines of water vapor located between 1.6 and 1.8 THz (see figure 2). Due to the large dynamic range of the spectrometer, the terahertz signal can be detected and analyzed even in the transmittance minimum at about 0.53 THz, see figure 5. The stronger absorption feature at 1.37 THz shows a still lower transmittance, see the inset of figure 4. In this case, our analysis yields reliable values of T down to 10^{-5}, in excellent agreement with the dynamic range of about 50 dB at 1.4 THz given in figure 2.

The lactose samples are pellets with near-parallel surfaces. Therefore, multiple reflections of the terahertz wave within the sample give rise to standing waves or Fabry–Perot interference fringes with maxima of order $\tilde{m}$ located at

$$\nu_{\tilde{m}} = \tilde{m}\,\frac{c}{2nd}. \tag{6}$$

In the transmittance spectrum shown in figure 4, the maxima can be observed up to $\tilde{m} = 13$. We find, e.g., $\nu_{10} = 857 \pm 4$ GHz; thus the optical thickness $n \times d$ is known with an accuracy

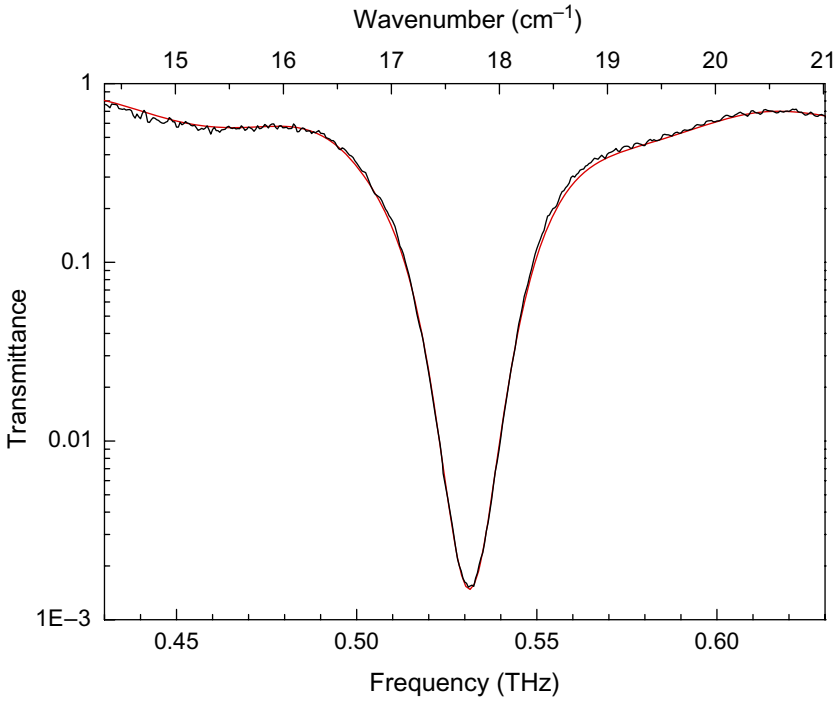

Figure 5. Transmittance of α-lactose monohydrate in the vicinity of the lowest absorption feature at 0.53 THz. The red line depicts a fit according to the Drude–Lorentz model.

of $\sim$0.5 %. In combination with the knowledge of $(n - n_{\mathrm{air}})d$ derived from the phase (see equation (4)), this allows us to determine the refractive index n directly from the optical data, without any further knowledge regarding d. The resulting frequency dependence of $n(\omega)$ is shown in figure 6. The typical line shape in the vicinity of an absorption feature is very well resolved even for the weak band at 1.195 THz. The additional small oscillations observed up to frequencies of about 1 THz are artifacts from the analysis based on equation (4), which assumes that the terahertz beam passes the sample only once, neglecting multiple reflections. These oscillations have the same period as the Fabry–Perot fringes observed in the transmittance, and they are observed in the same frequency range.

The effective thickness of the sample depends on the angle between the sample surface and the direction of propagation. In this case, the sample is placed in the collimated beam with the beam direction perpendicular to the sample surface. A finite angle of incidence would result in a slightly larger effective sample thickness. A not perfectly collimated beam (focused or divergent) can be taken into account by a thickness spread in equation (6). However, in our setup the divergence is less than 10° FWHM and therefore the effect on the thickness or equivalently on the refractive index is $\lesssim$1%, i.e. comparable to the accuracy given above. We have fitted the transmittance using the Drude–Lorentz model (see below). Allowing for a finite thickness spread did not improve the quality of the fit.

Below about 200 GHz, the error of both $T(\omega)$ and $n(\omega)$ increases, which is due to the enhanced importance of standing waves for large wavelengths.

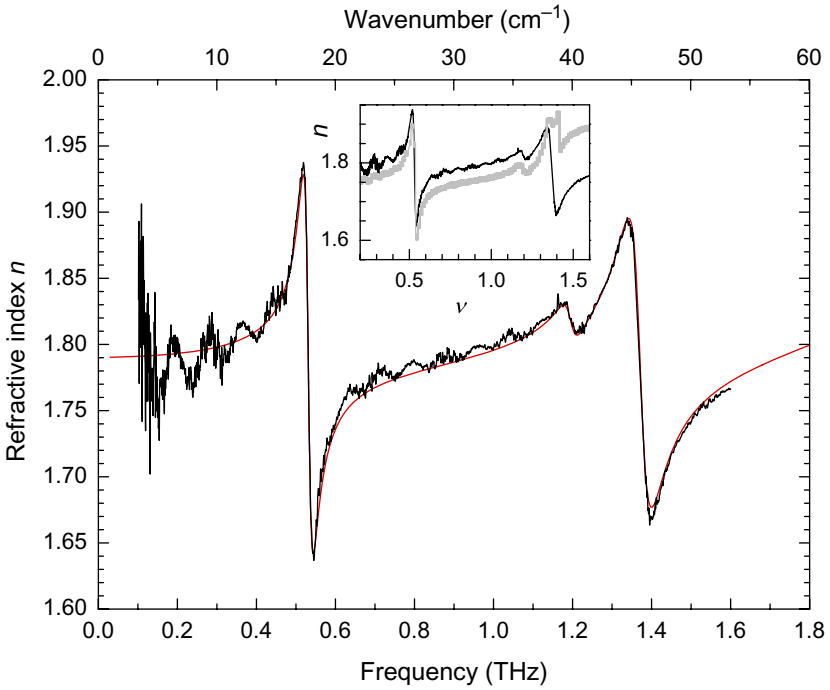

Figure 6. Refractive index n of α-lactose monohydrate as derived from the phase shift induced by the sample, see equation (4). The dispersion caused by the three absorption features at 0.530, 1.195 and 1.369 THz is very well resolved. The small oscillations are artifacts that arise because we neglect multiple reflections within the sample for the analysis of the phase. The red line depicts a fit according to the Drude–Lorentz model. Inset: comparison of our result for $n(\omega)$ (black line) with the data from Fischer [12] (gray) based on time-domain spectroscopy.

With the knowledge of the transmittance T and the refractive index n, we can calculate the extinction coefficient k (for $n \gg k$) by inverting (see e.g. [21])

$$T = \frac{(1-R)^2 \exp(-\alpha d)}{[1 - R\exp(-\alpha d)]^2 + 4R\exp(-\alpha d)\sin^2(n\omega \mathrm{d}/c)}, \tag{7}$$

with the absorption coefficient $\alpha = 2k\omega/c$, and the reflectance

$$R = \frac{(n-1)^2 + k^2}{(n+1)^2 + k^2}. \tag{8}$$

Finally, the dielectric function is obtained from

$$\varepsilon_1 = n^2 - k^2, \quad \varepsilon_2 = 2nk. \tag{9}$$

The final result for $\varepsilon_1(\omega)$ and $\varepsilon_2(\omega)$ is plotted in figure 7. As discussed above for $n(\omega)$, the three absorption lines are very well resolved, whereas the additional small oscillations in $\varepsilon_1(\omega)$ are artifacts of our analysis.

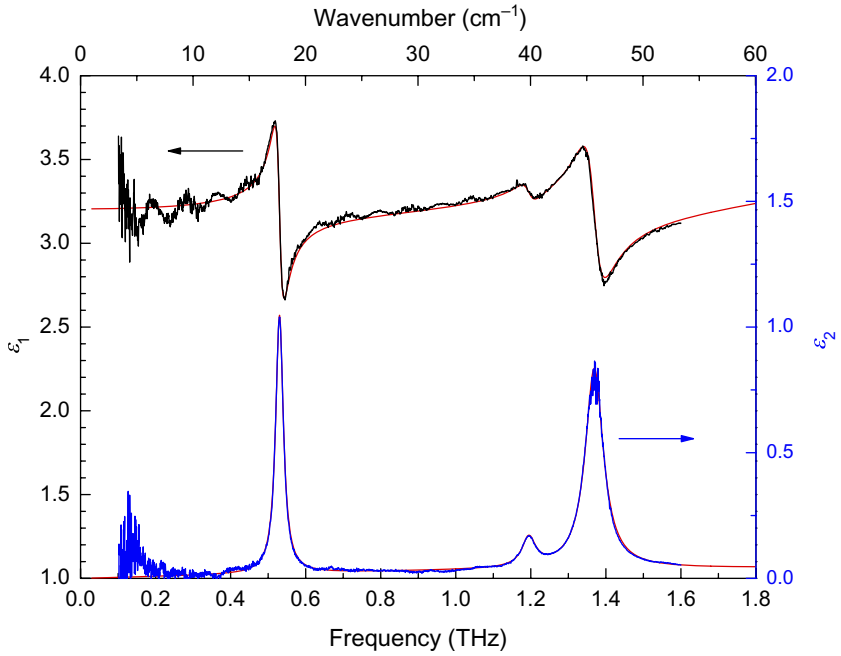

Figure 7. Real part $\varepsilon_1(\omega)$ (black, left axis) and imaginary part $\varepsilon_2(\omega)$ (blue, right axis) of the dielectric constant of α-lactose monohydrate. The red lines depict the results of the Drude–Lorentz model based on fitting $T(\omega)$ and $n(\omega)$; see figures 4 and 6.

Alternatively, one can obtain $\varepsilon_1(\omega)$ and $\varepsilon_2(\omega)$ by fitting $n(\omega)$ and $T(\omega)$ using a model dielectric function such as the Drude–Lorentz model

$$\varepsilon(\nu) = \varepsilon_\infty + \sum_i \frac{\nu_{p,i}^2}{\nu_i^2 - \nu^2 - \mathrm{i}\gamma_i \nu}, \tag{10}$$

where ν_i, $\nu_{p,i}$ and γ_i denote the center frequency, plasma frequency and the linewidth of the ith oscillator, respectively, and ε_∞ represents contributions from absorption features at high frequencies. The result of the simultaneous fit of $n(\omega)$ and $T(\omega)$ is shown in figures 4–7. All quantities are described very well, which clearly demonstrates the Kramers–Kronig consistency of our results. The logarithmic plot of $T(\omega)$ in figure 5 nicely shows that the absorption feature at 0.53 THz displays a perfect Lorentzian line shape (see [18] for comparison). Below 1.8 THz, our fit uses three oscillators with the following parameters:

$$\nu_1 = (530.4 \pm 0.5)\,\mathrm{GHz}, \quad \gamma_1 = (25 \pm 1)\,\mathrm{GHz},$$

$$\nu_2 = (1195 \pm 1)\,\mathrm{GHz}, \quad \gamma_2 = (44 \pm 3)\,\mathrm{GHz},$$

$$\nu_3 = (1369 \pm 2)\,\mathrm{GHz}, \quad \gamma_3 = (58 \pm 6)\,\mathrm{GHz}.$$

For the assignment of the different absorption lines we refer to density-functional calculations reported in [22, 23]. The overall suppression of $T(\omega)$ with increasing frequency is caused by phonons lying at higher frequencies [12]. We mimic their contribution in the fit with two oscillators located above 2.5 THz. Our results for the center frequencies ν_1, ν_2 and ν_3 are in very

good agreement with the data of different groups based on time-domain spectroscopy [12–17] and with the result of Brown *et al* [18] for ν_1 and γ_1 based on a frequency-multiplier chain. Note that the published results on ν_1 vary from 525 to 532 GHz [18] and very different values have been derived from time-domain spectroscopy, e.g. center frequencies of 0.58 and 1.51 THz [11], or a width $\gamma_1 = 69$ GHz [18]. The frequency dependence of the refractive index n has been reported by Fischer [12] on the basis of time-domain spectroscopy (see the inset of figure 6). The overall agreement with our result is very good; the absolute values agree within about 2%. This minor deviation is most probably due to uncertainties in the determination of the thickness d. The discrepancy above the absorption line at 1.369 THz is due to a phase jump, which has not been resolved in the time-domain data. In contrast, the results of [17] were obtained on a mixture of lactose and polyethylene, yielding a significantly smaller value of n and a reduced dispersion around the absorption lines.

Finally, we would like to contrast our results with the characteristics of well-established tools for spectroscopy of solid-state samples. Compared to other cw terahertz sources such as backward-wave oscillators (BWOs) or electronic sources with frequency-multiplier chains, the photomixing technique provides significantly less terahertz power but offers a much broader tuning range and a better beam quality (see e.g. [24, 25]). Using BWOs it is possible to cover the range from 36 GHz to 1.4 THz, but this necessitates the operation of about 12 different BWOs [24]. Fourier-transform spectrometers (Michelson type or Martin–Puplett type) span a very wide frequency range, for instance from the far-infrared to the UV (see e.g. [26, 27]). The lower frequency limit of commercially available spectrometers typically is in the range of 200 GHz–1 THz, with a maximum resolution of approximately 2–10 GHz. The signal-to-noise ratio at such low frequencies is poor. Determination of the complex dielectric function can be achieved by ellipsometry or by placing the sample within one of the arms of the interferometer. However, in a conventional measurement of the reflectance or transmittance, in most cases only the amplitude is determined, while the phase information is lost. The complex dielectric function then can be determined by extrapolating the data and employing a Kramers–Kronig analysis.

6. Conclusion

We have demonstrated that cw terahertz spectroscopy based on photomixing is excellently suited to determine the dielectric function $\varepsilon(\omega)$ of solid-state samples in a broad frequency range (60 GHz–1.8 THz). Homodyne detection preserves the phase information, enabling us to determine both $\varepsilon_1(\omega)$ and $\varepsilon_2(\omega)$ (or equivalently $n + \mathrm{i}k$) with high precision. Moreover, both the refractive index $n(\omega)$ and the sample thickness d can be determined independently, because the optical data yield both $(n-1)d$ and $n \times d$. Using the high spectral resolution (order of MHz) of the frequency-stabilized DFB laser diodes, we scan an interference pattern in frequency in order to avoid mechanically moving parts such as a delay stage, resulting in an effective frequency resolution of about 0.5 GHz for $\varepsilon(\omega)$. We presented precise data for the three lowest absorption lines of α-lactose monohydrate, making use of the large dynamic range of the terahertz power of up to 90 dB. Using a Drude–Lorentz fit, we have shown that our results are Kramers–Kronig consistent. Thus coherent broadband cw terahertz spectroscopy based on photomixing is a reliable alternative to time-domain or all-electronic techniques for studies of solid-state samples.

Acknowledgments

We express our gratitude to S Schindler for excellent experimental support. This work was supported by the DFG via SFB 608 and by the German Research Ministry BMBF ('Lynkeus' project; FSK 16SV2304).

References

[1] Matsuura S and Ito H 2005 *Terahertz Optoelectronics (Topics in Applied Physics* vol 97*)* ed K Sakai (Berlin: Springer) pp 157–202
[2] Lee Y S 2008 *Principles of Terahertz Science and Technology* (Berlin: Springer)
[3] McIntosh K A *et al* 1995 *Appl. Phys. Lett.* **67** 3844
[4] Verghese S *et al* 1998 *Appl. Phys. Lett.* **73** 3824
[5] Deninger A J *et al* 2008 *Rev. Sci. Instrum.* **79** 044702
[6] Sinyukov A M *et al* 2008 *Opt. Lett.* **33** 1593
[7] Göbel T *et al* 2009 *Electron. Lett.* **45** 65–6
[8] Mendis R *et al* 2005 *Int. J. Infrared Millim. Waves* **26** 201
[9] Mouret G *et al* 2006 *Appl. Phys. Lett.* **88** 181105
[10] Mouret G *et al* 2007 *Appl. Phys.* B **89** 395
[11] Taday P F 2004 *Phil. Trans. R. Soc.* A **362** 351
[12] Fischer B M 2005 *PhD Thesis* Albert-Ludwigs University, Freiburg, Germany
[13] Fischer B *et al* 2005 *Semicond. Sci. Technol.* **20** S246
[14] Walther M, Freeman M R and Hegmann F A 2005 *Appl. Phys. Lett.* **87** 261107
[15] Jung E *et al* 2008 *Biochip J.* **2** 296
[16] Byrne M B *et al* 2008 *Appl. Phys. Lett.* **93** 182904
[17] Withayachumnankul W, Fischer B M and Abbott D 2008 *Opt. Express* **16** 7382
[18] Brown E R *et al* 2007 *Appl. Phys. Lett.* **90** 061908
[19] Cámara Mayorga I *et al* 2007 *Appl. Phys. Lett.* **91** 031107
[20] Pickett H M *et al* 1998 *J. Quant. Spectrosc. Radiat. Transfer* **60** 883
[21] Klingshirn C F 1997 *Semiconductor Optics* (Berlin: Springer)
[22] Saito S *et al* 2006 *Japan. J. Appl. Phys.* **45** L1156
[23] Allis D G *et al* 2007 *Chem. Phys. Lett.* **440** 203
[24] Martens S, Gompf B and Dressel M 2009 *Appl. Opt.* **48** 5490
[25] Gorshunov B P *et al* 2005 *Int. J. Infrared Millim. Waves* **26** 1217
[26] Basov D N *et al* 2003 *Rev. Sci. Instrum.* **74** 4703
[27] Padilla W J *et al* 2004 *Rev. Sci. Instrum.* **75** 4710